Applied Catalysis B: Environmental 142–143 (2013) 654–661

Contents lists available at SciVerse ScienceDirect

Applied Catalysis B: Environmental

journal homepage: www.elsevier.com/locate/apcatb

Photocatalytic decomposition of perfluorooctanoic acid in pure water and sewage water by nanostructured gallium oxide☆

Tian Shao, Pengyi Zhang*, Ling Jin, Zhenmin Li

State Key Joint Laboratory of Environment Simulation and Pollution Control, School of Environment, Tsinghua University, Beijing 100084, China

ARTICLE INFO

Article history:
Received 5 February 2013
Received in revised form 30 May 2013
Accepted 31 May 2013
Available online 10 June 2013

Keywords:
Gallium oxide
Sheaf-like structure
Perfluorooctanoic acid
Photocatalysis
Vacuum ultraviolet

ABSTRACT

Due to its global occurrence and environmental persistence, perfluorooctanoic acid (PFOA) has attracted worldwide concerns including its decomposition method. The nanostructured β-Ga_2O_3 with a novel sheaf-like structure was synthesized via a PVA-assisted hydrothermal method and subsequent heat treatment. The sheaf-like Ga_2O_3 was self-assembled from nanoplates, possessing a high value of specific surface area (36.1 m^2/g) and a large number of nanopores (2–4 nm and 8 nm). Sheaf-like Ga_2O_3 exhibited a remarkable photocatalytic activity for PFOA decomposition in pure water under 254 nm UV irradiation with the rate constant of 4.85 h^{-1}, which was 16 and 44 times higher than that of commercial Ga_2O_3 and P25 respectively. This can be attributed to the close bonding between PFOA and Ga_2O_3, and nanoporous structure of sheaf-like Ga_2O_3. In addition, in combination of 185 nm vacuum UV irradiation, the sheaf-like Ga_2O_3 showed high efficiency to remove trace PFOA in the secondary effluent of sewage, in which the decomposition of targeted trace pollutants such as PFOA is generally inhibited by coexisting high-level natural organic matters and bicarbonate.

© 2013 Elsevier B.V. All rights reserved.

1. Introduction

Perfluorooctanoic acid (PFOA, $C_7F_{15}COOH$) is an emerging persistent organic pollutant belongs to a class of fully fluorinated hydrocarbons known as perfluorocarboxylic acids (PFCAs, $C_nF_{2n+1}COOH$). Due to the strong carbon–fluorine bonds, PFOA is extraordinary thermally, chemically stable and surface active, hence it is widely used as surfactant and fire retardant in various industrial fields for the past decades. As a result, PFOA and its precursors have been released into the nature particularly from wastewater treatment plants [1]. Due to its environmental persistence and bioaccumulation, it has been extensively reported that PFOA is globally distributed in waters, animals and humans [2–4]. Toxicological studies demonstrated that exposure to PFOA could lead to developmental and reproductive toxicities, liver damage and possibly cancer [5,6]. The potential hazard PFOA posed to the human health and wild life has increasingly attracted worldwide concerns, therefore, the developments for PFOA decomposition technologies are much required.

PFOA resists most conventional treatment processes including biological degradation, oxidation and reduction [7]. The recent studies show that some special techniques can decompose PFOA in aqueous solution, such as high-frequency ultrasonication [8], ultraviolet irradiation [9], periodate photolysis [10], persulfate photolysis [11] and KI photolysis [12], phosphotungstic-acid [13] and Fe(II)/Fe(III) photocatalysis [14]. However, together with the relatively low decomposition efficiency and severe reaction conditions, most of these researches were carried out in pure aqueous solutions and concentrations of PFCAs are much higher than those found in actual contaminated waters and discharge sources of PFOA, which generally ranges from ng/L to μg/L [1]. The real wastewater contains various inorganic and organic matters, and these coexisting constituents do inhibit PFOA photolysis, as well as decrease the sonochemical degradation of PFOA by consuming energy and competitive adsorption [15,16]. Therefore, how to effectively decompose PFOA in real water is still a difficult problem to overcome.

Among potential methods for PFOA decomposition, heterogeneous photocatalysis is attractive for its low energy consumption and high efficiency to completely degrade various kinds of organic contaminants. However TiO_2, the most widely used photocatalyst, showed very low activity for PFOA decomposition in mild condition [17]. Fortunately, other semiconductor materials are proved to possess activity to decompose PFOA, such as β-Ga_2O_3 [18] and In_2O_3 [19]. And their activity can be further enhanced through proper synthetic strategy to obtain nanostructured materials

☆ This is an open-access article distributed under the terms of the Creative Commons Attribution-NonCommercial-No Derivative Works License, which permits non-commercial use, distribution, and reproduction in any medium, provided the original author and source are credited.

* Corresponding author. Tel.: +86 10 62796840; fax: +86 10 62797760.
E-mail address: zpy@tsinghua.edu.cn (P. Zhang).

0926-3373/$ – see front matter © 2013 Elsevier B.V. All rights reserved.
http://dx.doi.org/10.1016/j.apcatb.2013.05.074

because the structure, morphology and size of materials can significantly influence their properties and application. Li et al. [20] reported that nanoporous In_2O_3 nanospheres showed excellent photocatalytic activity under UV irradiation to decompose PFOA in pure water. This result implies that photocatalysts with novel nanostructures can gain higher efficiency in decomposing PFOA.

β-Ga_2O_3 is a wide bandgap semiconductor (E_g = 4.8 eV) [18] that finds versatile applications in optoelectronic devices, high temperature electronic devices and high temperature stable gas sensors [21,22]. Diverse nanostructures of Ga_2O_3 have been synthesized, such as nanowires, nanobelts, nanosheets and nanoplates [23,24]. Here, we synthesize Ga_2O_3 nanomaterials with a novel nanostructure, i.e. sheaf-like, which, to the best of our knowledge, is first reported. The sheaf-like β-Ga_2O_3 is prepared via a PVA-assisted hydrothermal method followed by calcination. The as-prepared materials exhibited remarkable photocatalytic activity for decomposition of PFOA in pure water under mild conditions. Though in municipal wastewater, the efficiency decreased due to the presence of bicarbonate and organic matters, it can be almost completely rectified by slight pH adjustment and using 185 nm UV to replace 254 nm UV irradiation.

2. Experimental

2.1. Preparation of sheaf-like Ga_2O_3

All reagents (purchased from Beijing Chemical Co., Ltd.) were analytical grade and were used as received. Sheaf-like Ga_2O_3 were synthesized with a hydrothermal method followed by calcination. In a typical procedure, 2 g (5 mmol) of $Ga(NO_3)_3{\cdot}xH_2O$ and 0.1173 g PVA was dissolved in 20 mL of pure water. After heated at 90 °C in a circulator for 15 min, the mixture was transferred into a 25-mL Teflon-lined stainless steel autoclave and maintained at 200 °C for 8 h. After the autoclave was cooled to room temperature naturally, the white precipitates (precursor of Ga_2O_3) were collected by centrifugation, and then washed with pure water and ethanol for several times. Ga_2O_3 powder was obtained from the precursor via calcination at 700 °C for 2 h in nitrogen (heating rate 1 °C/min).

2.2. Characterization

X-ray powder diffraction (XRD) patterns were taken on PAnalutical X'Perpro diffractometer at 40 kV voltage and 30 mA current. Transmission electron microscopy (TEM) images were taken on a JEM 2010F microscope at 200 kV accelerating voltage. The morphologies of the samples were observed using an ultra high-resolution field-emission scanning electron microscope (FESEM, S-5500, Hitachi) performed at 30 kV accelerating voltage. N_2 adsorption–desorption isotherms were obtained on a Micromeritics ASAP 2000 instrument.

Electron spin resonance (ESR) signals of radicals trapped by DMPO were recorded on a Bruker A-300 spectrometer at ambient temperature under irradiation of a mercury lamp (ER-203UV, 100 W). Measurements of diffuse reflectance infrared Fourier transform spectroscopy (DRIFTS) were carried out on a Nicolet NEXUS 670-FTIR spectrometer equipped with a smart collector and an MCT detector cooled by liquid N_2. The IR spectra were recorded by accumulating 100 scans at a resolution of 4 cm^{-1}.

2.3. Photocatalytic decomposition of PFOA

The photocatalytic decomposition of PFOA was conducted in a tubular quartz vessel reactor under ultraviolet irradiation. Two kinds of low-pressure mercury lamps (14 W, Cnlight Co. Ltd, China) with same electric power and appearance size were alternatively used. One only emits 254 nm UV light (hereafter referred as UV), and the other emits 254 nm UV and 185 nm vacuum UV light (hereafter referred as VUV). One UV or VUV lamp was placed in the center of the reactor with two-layer quartz tubes protection. In a typical experiment, 150 mL of PFOA aqueous solution ($C_0 \approx 500$ μg/L) was prepared by diluting the stock solution in a beaker. The diluting water could be pure water or secondary effluent taken from a municipal wastewater treatment plant. 0.075 g of photocatalyst (0.5 g/L) was added in PFOA solution and stirred for 0.5 h. Then, the suspension was added into the reactor and continuously bubbled with oxygen gas at a flow rate of 80 mL/min. Then the lamp was turned on and the reaction temperature was maintained at 25 °C with a cooling water jacket around the reactor. At a regular time interval, aliquots of sample were taken and filtered with 0.22 μm ultrafiltration membrane to remove photocatalyst powder. To avoid possible impact of filter adsorption on PFOA concentration, the first 3 mL of filtrate was discarded.

2.4. Analyses

Concentrations of PFOA and its decomposition products were measured on a Waters Acquity UPLC system, coupled with a Micromass Quattro Premier tandem quadrupole mass spectrometer (Waters, Milford, USA). The multiple reaction monitoring mode (MRM) was used for quantitative analysis of PFOA and other shorter-chain PFCAs. The separation column was a Waters Acquity UPLC BEH C_{18} column (2.1 mm i.d. × 50 mm, 1.7 μm particles), and the column temperature was set at 50 °C. The flow rate was maintained at 0.4 mL/min with a mobile phase of eluent A (2 mmol/L ammonium acetate/methanol) and B (2 mmol/L ammonium acetate/water). The eluent gradient started with 30% A for 0.5 min, then was linearly increased to 90% A in 4.5 min, and further increased to 100% A in 1 min and finally back to 30% A in 3 min. MS detection was operated in negative mode by using an electrospray source. The optimum mass parameters obtained were as follows: capillary voltage, 2.1 kV; source temperature, 120 °C; desolvation temperature, 280 °C; and desolvation gas flow rate, 650 L/h. The parent ion, daughter ion, cone voltage (V), and collision energy (eV) for PFCAs detection were PFOA (413 > 369, 17, 11), PFHpA (363 > 319, 16, 10), PFHxA (313 > 269, 15, 10), PFPeA (263 > 219, 15, 10), PFBA (213 > 169, 12, 10), PFPrA (163 > 119, 12, 10) and TFA (113 > 69, 12, 10), respectively.

The concentration of F^- was determined by a Dionex ion chromatography (ICS-2000, USA). Sample was injected into an IonPac AS11-HC column (250 mm × 4 mm) with an IonPac AG11-HC guard column (50 mm × 4 mm). A mixture solution containing 3.2 mM Na_2CO_3 and 1 mM $NaHCO_3$ as the mobile phase was delivered with a flow rate of 1.0 mL/min.

3. Results and discussion

3.1. Crystal phase and microstructure of Ga_2O_3

The XRD patterns of samples synthesized by a PVA-assisted hydrothermal process at 200 °C for 8 h are shown in Fig. 1(a). All the peaks can be well indexed to α-GaOOH (JCPDS, No. 06-0180) with no observation of other impurities. The peaks are sharp and narrow, indicating high crystallinity of samples. After calcined at 700 °C in nitrogen for 2 h, the as-synthesized α-GaOOH crystals were transformed to pure monoclinic β-Ga_2O_3 (JCPDS, No. 41-1103), as shown in Fig. 1(b).

Fig. 2(a) and (b) is typical SEM images of as-synthesized GaOOH, indicating that the sample possesses a special morphology, which seems that a bundle of platy crystals are bandaged in its middle, with the top and bottom fanning out while the middle remaining thin and hence is named as "sheaf structures" [25]. While the

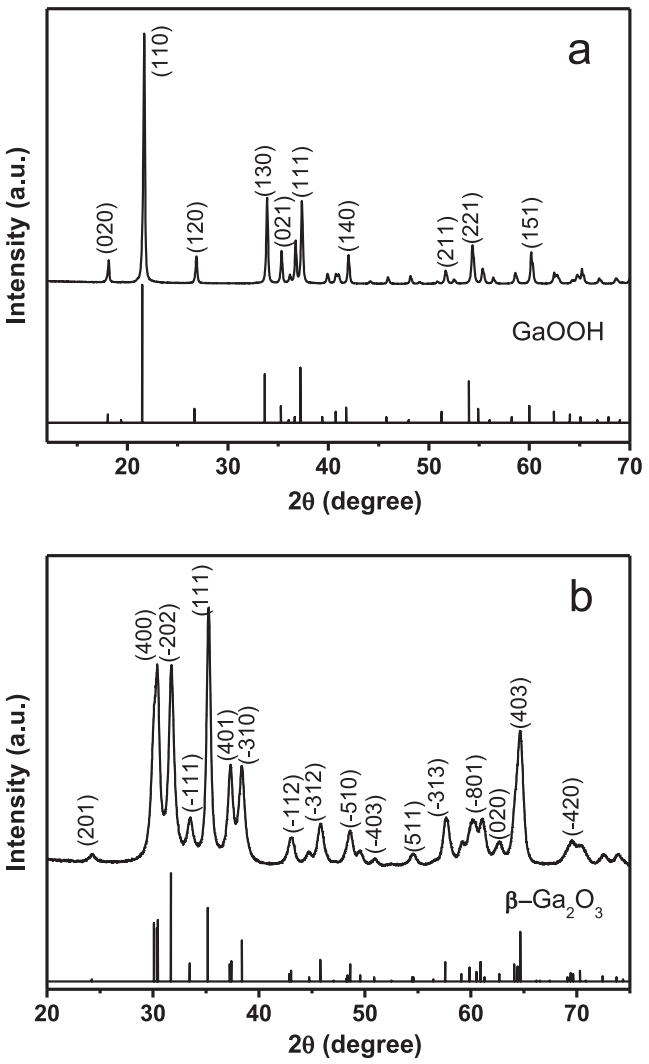

Fig. 1. XRD patterns of (a) the obtained GaOOH and (b) Ga_2O_3 samples.

double-sheaf morphology dominates in the obtained samples, half-sheaf structures with a V-shape are also observed. Further observation from the high-magnification SEM images shows that the individual sheaf has a length in the range of 2–3 μm and a middle diameter in the range of 0.5–1 μm. The individual nanoplate has an average width of 100 nm and thickness of 10 nm. Upon calcination at 700 °C for 2 h in nitrogen, as-obtained Ga_2O_3 product almost remains the morphology and architecture of its precursor, as show in Fig. 2(c). However, Fig. 2(d) shows the surface of material become rough due to the dehydration shrinkage during calcination.

Such self-assembled shelf-like structure of Ga_2O_3 was further observed with TEM. Close examination of TEM image shown in Fig. 3(a) indicates that sheaf-like Ga_2O_3 consists of numerous nanoplates radially fanning out from the center of the structure. Each nanoplate is about 80–100 nm in width and 1–1.5 μm in length, and dense nanopores in the nanoplate can be clearly observed. The inset of Fig. 3(a) shows the select area electron diffraction (SAED) pattern of an individual nanoplate, the presence of obvious discrete spots reveals its single-crystalline feature. A high-magnification TEM image (Fig. 3(b)) of a nanoplate segment (marked in the inset of Fig. 3(b)) shows clear lattice fringe with lattice interplanar spacing of 0.296 nm, which corresponds to (4 0 0) crystal plane of β-Ga_2O_3. The lattice fringes reveal that the nanoplates are elongated in the [1 0 0] direction.

The N_2 adsorption–desorption isotherm of sheaf-like Ga_2O_3 is shown in Fig. 4. The isotherm is identified as type IV with hysteresis loop, indicating that the sample contained mesopores in the structure. The pore-size distribution (inset of Fig. 4) obtained from the isotherm indicates the existence of a number of nanopores (2–4 nm), which may correspond to those observed in nanoplates with TEM. These small pores may arise from the loss of the adsorbed PVA molecule and dehydration shrinkage during the conversion process from GaOOH to Ga_2O_3. The large pores (5–13 nm) may arise from the stack of nanoplates. The BET specific surface area of as-synthesized sheaf-like Ga_2O_3 was 36.1 m^2/g, while that of commercial Ga_2O_3 was 11.5 m^2/g.

3.2. UV photocatalysis of PFOA in pure water and its mechanism

A series of comparative experiments were carried out to investigate the photocatalytic activity of sheaf-like Ga_2O_3, commercial Ga_2O_3, P25 TiO_2 for decomposition of PFOA in pure water. The aqueous solution of PFOA (500 μg/L) was irradiated with a 254 nm UV lamp. The initial pH value of the PFOA solution was about 4.7, which was not adjusted during the whole process. As shown in Fig. 5(a), the direct photolysis of PFOA by 254 nm UV light was very slow and can be neglected. PFOA decomposition by using P25 TiO_2 was also insignificant under this mild condition. Besides 3% PFOA was adsorbed, only 20% PFOA was decomposed within 3 h. In the presence of commercial Ga_2O_3, about 6% PFOA was adsorbed, and the decomposition ratio of PFOA within 3 h increased to 38%, which was about two times higher than that by P25 TiO_2. However, when as-synthesized sheaf-like Ga_2O_3 was used as photocatalyst, adsorption ratio was 10%, and the decomposition rate of PFOA increased dramatically, PFOA completely decomposed within 45 min. The PFOA decomposition under various conditions fitted well with pseudo-first-order kinetics. The rate constant of sheaf-like Ga_2O_3 was 4.85 h^{-1}, which was nearly 16 and 44 times higher than that of commercial Ga_2O_3 (0.30 h^{-1}) and P25 TiO_2 (0.11 h^{-1}) respectively. It is apparent that, nanostructured sheaf-like Ga_2O_3 shows great photocatalytic activity for PFOA decomposition, with higher decomposition rate than other methods such as photochemical decomposition and sonolysis [26].

Besides the fluoride ion was detected as the final product of PFOA decomposition, C2–C7 shorter-chain PFCAs were identified as major intermediate products by UPLC-MS/MS. The time-dependant change of intermediates and fluoride ion during PFOA decomposition is given in Fig. 5(b). The amount of C7 PFCA, i.e. PFHpA increased to a maximum within 30 min and then gradually decreased. PFHxA followed a similar trend, except that the time reaching a maximum concentration was 60 min. Concentrations of other shorter-chain PFCAs were low, though they increased during the 3 h of reaction. And the shorter the carbon chain is, the lower its concentration is. These characteristics strongly suggest stepwise cleavage of PFOA carbon-chain during its photocatalytic decomposition. Simultaneously, fluoride ion in aqueous solution was detected and increased with time. After 3 h of reaction, the defluorination ratio reached 61%, which was slightly lower than expected, fluoride ions may adsorb on the photocatalyst surface which was positively charged at acidic pH value during the reaction.

The excellent performance of as-synthesized Ga_2O_3 for PFOA decomposition can be attributed to the unique bonding to PFOA and its special sheaf-like nanostructure. As previous research showed, the fully fluorinated structure of PFOA molecule makes it inert to $^{\bullet}OH$ radical attack [26,27], thus reaction with photogenerated holes seems to be the dominant pathway for PFOA decomposition. Fig. 6 is the spectrum of ESR trapped with *5,5*-dimethyl-*1*-pyrroline N-oxide (DMPO), which was carried out on illuminated PFOA solution containing different photocatalysts. Four characteristic peaks of DMPO-$OH^{\bullet}$ adducts could be clearly observed in the suspension of

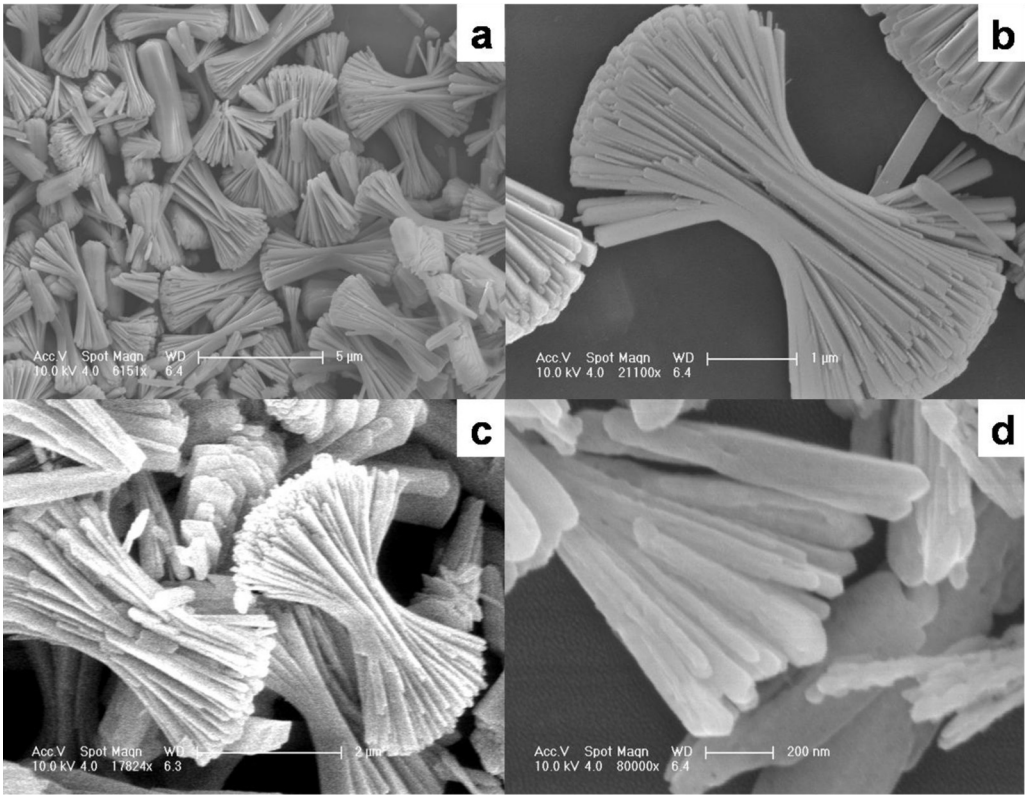

Fig. 2. (a) Low- and (b) high-magnification FESEM images of as-synthesized α-GaOOH and (c) (d) β-Ga_2O_3.

TiO_2 and Ga_2O_3 respectively. However, the peak intensities for TiO_2 were much stronger than those for Ga_2O_3. This result indicates that the photogenerated holes in TiO_2 preferentially react with water or hydroxide to form hydroxyl radicals, while those in Ga_2O_3 tend to react with PFOA directly.

This difference between Ga_2O_3 and TiO_2 can be attributed to their different modes bonding to PFOA. As shown in DRIFTS spectra of PFOA adsorbed on Ga_2O_3 and TiO_2 (Fig. 7), the peaks in the range of 1690–1600 cm^{-1} are assigned to asymmetric stretches ($\nu_{as}(COO^-)$) of carboxylate, while the peaks in the range of 1500–1400 cm^{-1} are assigned to symmetric stretches ($\nu_s(COO^-)$) of carboxylate [28–30]. Concluded by Deacon et al. [31], the value of $\Delta\nu$, i.e. $\nu_{as}(COO^-)$–$\nu_s(COO^-)$ reflects the coordination mode between carboxylate and cation. The $\Delta\nu$ value which substantially greater than the ionic $\Delta\nu$ indicates a unidentate coordination, while the $\Delta\nu$ value which is significantly less than the ionic $\Delta\nu$ indicates a bidentate or bridging coordination. The $\Delta\nu$ value for PFOA/TiO_2 (278 cm^{-1}) is substantially greater than that of K^+ salt (203 cm^{-1}), which indicates that PFOA coordinates to TiO_2 in a unidentate mode. While the $\Delta\nu$ value for PFOA/sheaf-like Ga_2O_3 (191 cm^{-1}) and that for PFOA/commercial Ga_2O_3 (196 cm^{-1}) is smaller than the ionic $\Delta\nu$, it can be concluded the terminal carboxylate group of PFOA molecule tightly coordinates to the Ga_2O_3 surface in a bidentate or bridging configuration, which is beneficial for PFOA to be

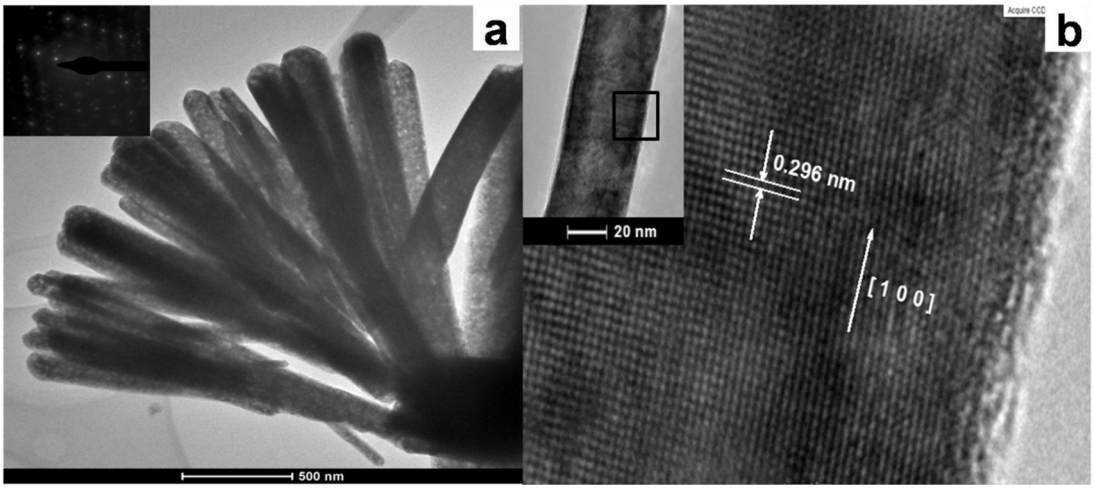

Fig. 3. (a) TEM image of sheaf-like Ga_2O_3 and the corresponding SAED pattern (inset in the upper left corner). (b) HRTEM image of a nanoplate segment (inset in the upper left corner) of sheaf-like Ga_2O_3.

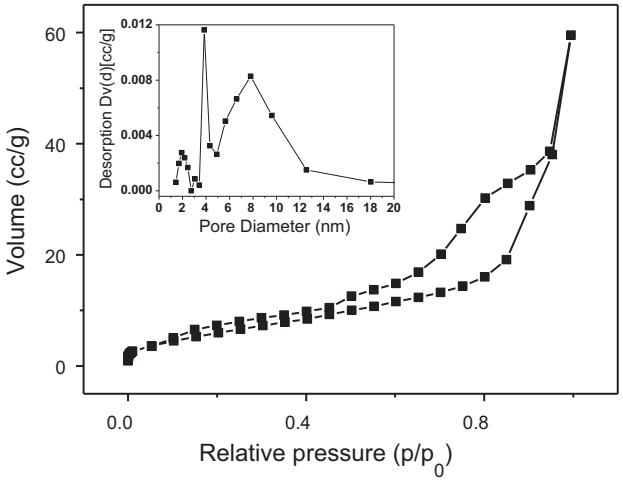

Fig. 4. Nitrogen adsorption–desorption isotherm of sheaf-like Ga_2O_3. The inset is Barrett–Joyner–Halenda (BJH) pore size distribution curve.

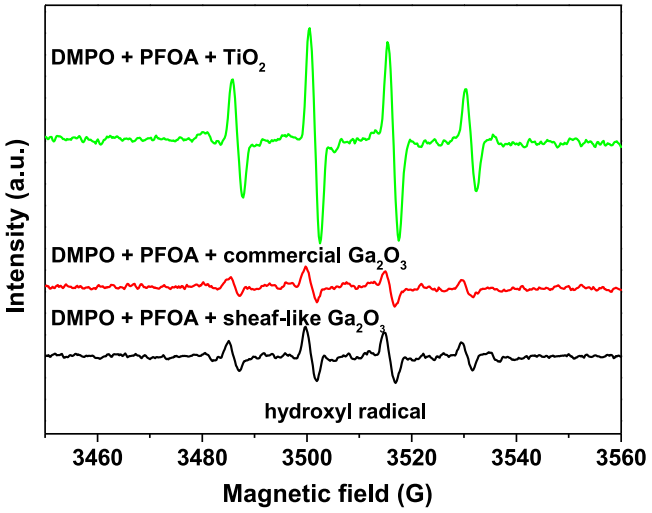

Fig. 6. DMPO spin-trapping ESR spectra of PFOA solution under UV irradiation for 4 min at room temperature in the presence of Ga_2O_3 or TiO_2.

directly decomposed by photogenerated holes of Ga_2O_3 under UV irradiation. Thus compared to TiO_2, both commercial and sheaf-like Ga_2O_3 exhibited better photocatalytic activity for PFOA decomposition.

It is worth noting that compared to commercial Ga_2O_3, the sheaf-like Ga_2O_3 showed remarkable photocatalytic activity. Together with the enlarged surface area, interface between nanoplates in the sheaf structure can provide more adsorption and reaction centers, thus it has a beneficial effect on the activity of catalysts. In addition, the sheaf-like Ga_2O_3 consisted of nanoplates elongating in the [1 0 0] direction, thus the nanoplates exposed a predominant crystal facet. Recently, it is extensively reported that TiO_2 with exposed (0 0 1) facets shows much higher activity and selectivity than those without predominant facets [32,33]. Similarly, it is reasonable that, the sheaf-like Ga_2O_3 with predominant facet shows better activity than other Ga_2O_3 materials. Meanwhile, the obtained sheaf-like Ga_2O_3 was calcined in nitrogen atmosphere, which may increase oxygen vacancy and oxygen-ionic conductivity [34] and accordingly favors the photocatalysis of PFOA.

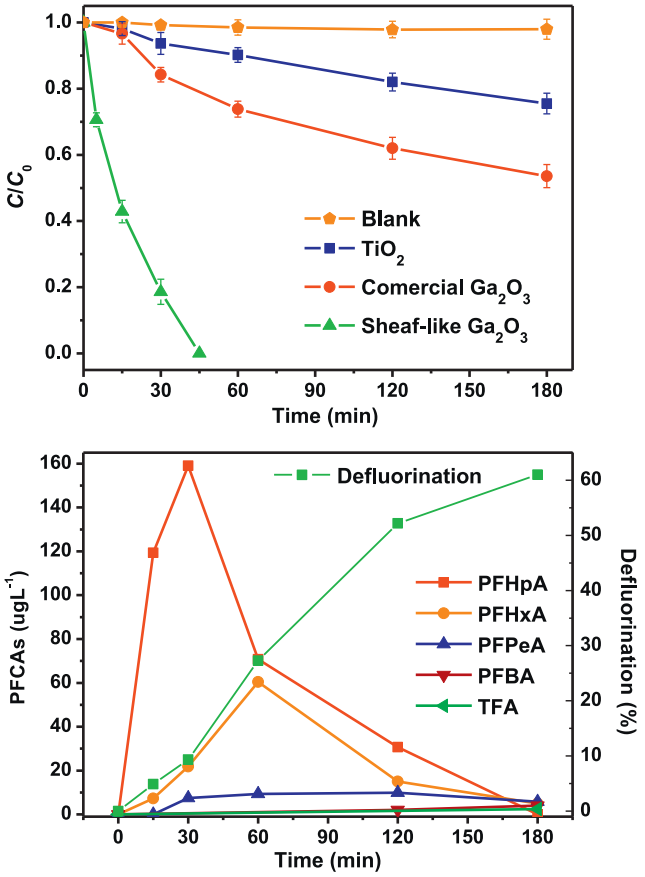

Fig. 5. (a) Time dependence of PFOA in pure water under UV irradiation in the presence various photocatalysts; and (b) time dependence shorter-chain intermediates and defluorination in the presence of sheaf-like Ga_2O_3. The initial pH value was 4.7.

3.3. UV photocatalysis of PFOA in sewage water

To validate the feasibility of sheaf-like Ga_2O_3 photocatalysis to decompose PFOA in a real wastewater, in which coexisting

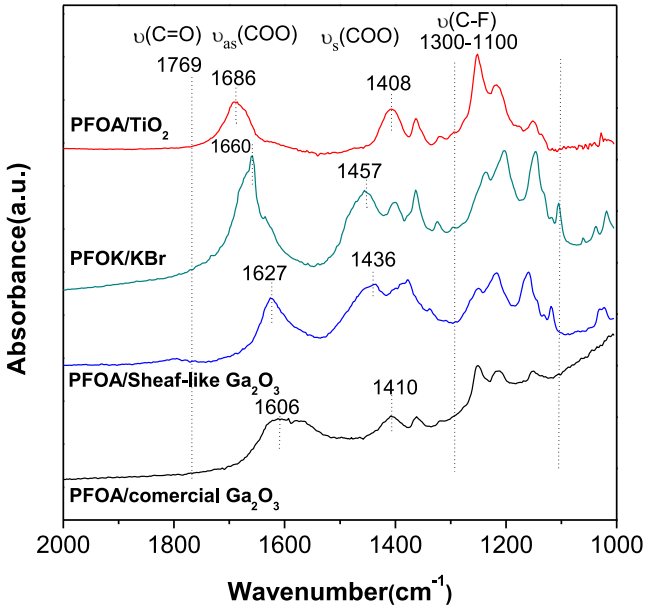

Fig. 7. DRIFT spectra of PFOA mixed with KBr and adsorption-equilibrium on Ga_2O_3 and TiO_2 photocatalysts at room temperature. The samples of PFOA/photocatalyst were filtered and dried at room temperature for 24 h before measurement.

Table 1
Characteristics of the secondary effluent taken from a municipal wastewater plant in Beijing, China.

Parameter	Value	Parameter	Value
TOC	18.9 mg/L	pH	7.80
Bicarbonate	4.76 mmol/L	Na^+	81.8 mg/L
TDS	452 mg/L	K^+	14.6 mg/L
F^-	0.28 mg/L	Mg^{2+}	30.0 mg/L
Cl^-	107 mg/L	Ca^{2+}	85.7 mg/L
SO_4^{2-}	108 mg/L	Mn	0.08 mg/L
NO_3^-	40.2 mg/L	Fe	<0.03 mg/L

Table 2
Decomposition rate and half-life of PFOA in sewage water under UV or VUV irradiation.

Light source	Blank	P25 TiO_2	Commercial Ga_2O_3	Sheaf-like Ga_2O_3	
	pH 4.3	pH 4.3	pH 4.3	pH 4.3	pH 7.8
UV					
k (h^{-1})	–	0.09	0.10	1.43	1.00
$t_{1/2}$ (h)	–	8.06	6.59	0.483	0.69
VUV					
k (h^{-1})	1.21	0.98	1.39	4.29	1.95
$t_{1/2}$ (h)	0.57	0.70	0.50	0.16	0.35

compounds may reduce decomposition efficiency, we investigated the decomposition of PFOA added in a secondary effluent (its composition is listed in Table 1) taken from a municipal wastewater plant in Beijing, China.

Fig. 8 shows the time-dependent change of PFOA in wastewater, and the experiment conditions were the same as those in pure water (Fig. 5(a)). In the original secondary effluent with pH of 7.8, the decomposition of PFOA was obviously retarded, and only 81% of PFOA was decomposed within 3 h in the presence of sheaf-like Ga_2O_3. The rate constant was reduced to 1.00 h^{-1} (Table 2), only 21% of that in pure water (4.85 h^{-1}). Similarly, the decomposition rate of PFOA in the presence of commercial Ga_2O_3 or P25 TiO_2 was also reduced.

The lower decomposition rate of PFOA in the secondary effluent can be attributed to the influence of bicarbonate and organic matters. Bicarbonate (HCO_3^-) has the same carboxyl group as PFOA, and its concentration (4.76 mmol/L) was nearly 3000 times higher than PFOA concentration added in the secondary effluent,

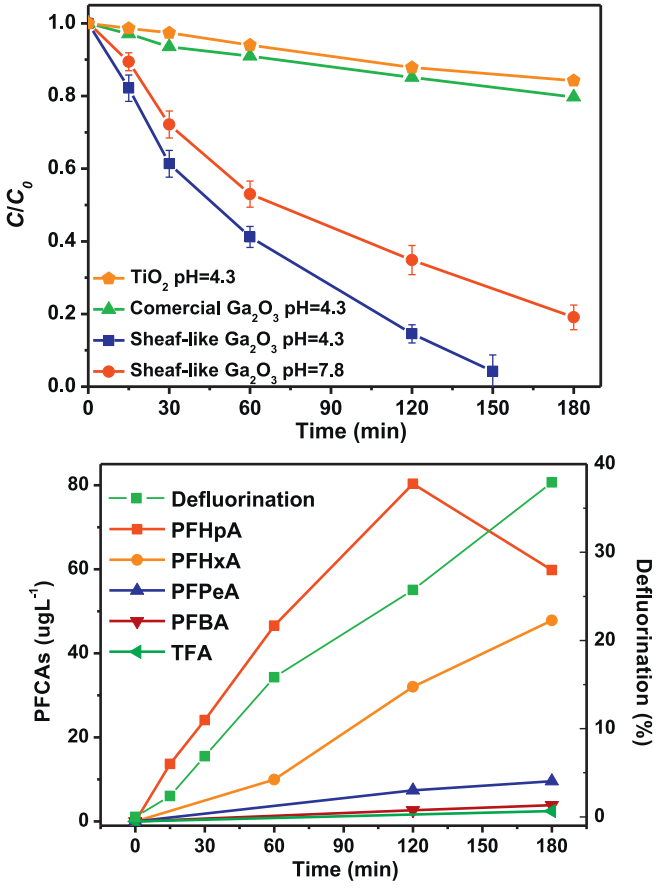

Fig. 8. Time dependence of PFOA in sewage water under UV irradiation in the presence of various photocatalysts. The original pH of sewage water was 7.8 and was adjusted to 4.3 with HCl.

the competitive adsorption of bicarbonate on the surface of Ga_2O_3 inhibited the adsorption of PFOA, thus reducing its decomposition efficiency [19]. After the pH value of the secondary effluent was adjusted to 4.3, making bicarbonate transformed into carbonic acid, the percentage of PFOA decomposed increased from 81% to 100% after 3 h of reaction. However, PFOA decomposition was still greatly delayed compared to that in pure water, reflecting the impact of organic matters in the secondary effluent, which may also competitively adsorb and attenuate UV penetration in water [19].

3.4. VUV photocatalysis of PFOA in sewage water

Considering the synergistic effect of VUV irradiation on photocatalyst and its ability to eliminate natural organic matters [35,36], combination of Ga_2O_3 with VUV irradiation was used for degradation of PFOA in wastewater. The wastewater solution of PFOA (500 μg/L) was irradiated with a 185 nm VUV lamp in the presence of sheaf-like Ga_2O_3, commercial Ga_2O_3, or P25 TiO_2. To avoid the effect of bicarbonate, the pH was adjusted to 4.3 with HCl. The blank experiment, i.e. direct VUV photolysis, was carried out at the same condition without photocatalyst.

Since PFOA has a strong absorption from deep UV region to 200 nm [13], VUV irradiation itself can cause decomposition of PFOA. As shown in Fig. 9(a), by direct VUV photolysis, 92% of initial PFOA was decomposed after 3 h of irradiation, which was in agreement with the result of Chen et al. [37]. Using the sheaf-like Ga_2O_3 in combination of VUV irradiation, the rate of PFOA decomposition was significantly enhanced, and 100% of initial PFOA decomposed within 65 min. As shown in Table 2, the decomposition rate constants of PFOA in wastewater for sheaf-like Ga_2O_3/VUV, was 4.29 h^{-1}, which was almost recovered to that by sheaf-like Ga_2O_3/UV in pure water (4.85 h^{-1}). The time-dependant change of products during PFOA decomposition in wastewater by sheaf-like Ga_2O_3/VUV is shown in Fig. 9(b), which is similar to that in pure water by sheaf-like Ga_2O_3/UV. No other products other than F^- and shorter-chain PFCAs were detected, and the defluorination ratio of PFOA was up to 66%, which was 2.27 times higher than that by VUV photolysis (29%).

The stability of sheaf-like Ga_2O_3 catalyst was tested by repeating the photocatalytic decomposition of PFOA. PFOA-containing wastewater solution (500 μg/L) was irradiated with 185 nm VUV lamp in the presence of the sheaf-like Ga_2O_3 (0.5 g/L). Before each cyclic test, same amount of PFOA was added into the solution to make sure the initial concentration of PFOA was same. As shown in Fig. 10, PFOA was almost totally decomposed with 60 min in all 3 cycles. The residual PFOA in the third round seems slightly higher than the first round. This can be attributed to the effects of residual intermediate PFCAs, which was not completely decomposed within 60 min as shown in Fig. 9(b).

The high efficiency and good stability of the sheaf-like Ga_2O_3/VUV process for PFOA removal from real wastewater is not only contributed by VUV irradiation, which eliminates adverse

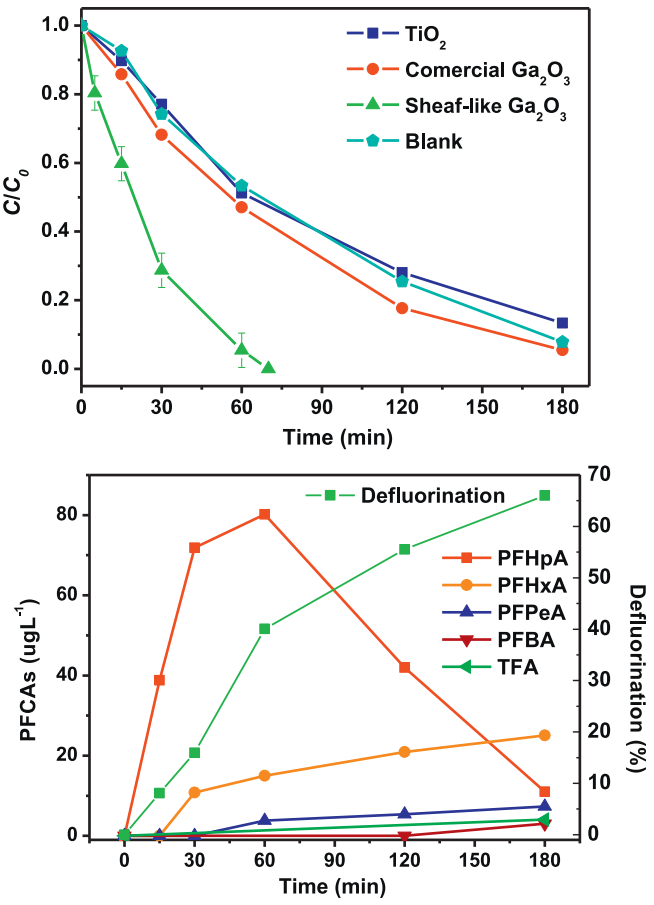

Fig. 9. (a) Time dependence of PFOA in sewage water under VUV irradiation in the presence of various photocatalysts; and (b) time dependence of shorter-chain intermediates and defluorination in the presence of sheaf-like Ga_2O_3. The initial pH value was 4.3.

impacts of coexisting organic matters, but also attributed to the unique role of nanostructured Ga_2O_3 to decompose PFOA. When P25 TiO_2 or commercial Ga_2O_3 was used to replace sheaf-like Ga_2O_3 under VUV irradiation, as shown Fig. 9(a), no significant improvement occurred compared with VUV direct photolysis. This further demonstrates the important role of nanostructured Ga_2O_3 as photocatalyst to guarantee high efficiency in decomposing PFOA in sewage water.

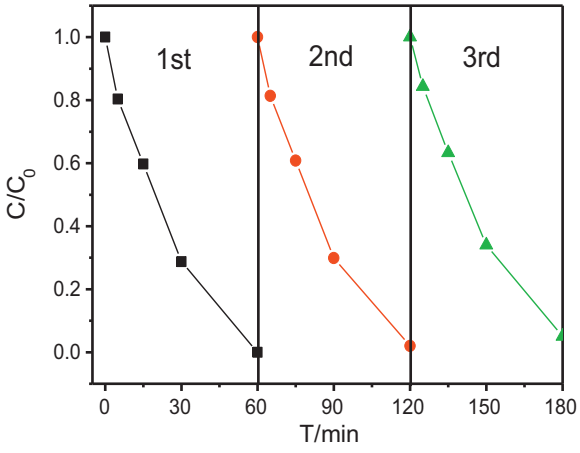

Fig. 10. Time dependence of PFOA in sewage water under VUV irradiation in the presence of sheaf-like Ga_2O_3 in 3 cyclic tests.

4. Conclusion

A novel β-Ga_2O_3 with sheaf-like nanostructure was synthesized through a hydrothermal method followed by calcination. The sheaf-like Ga_2O_3 consisted of nanoplates elongating in the [1 0 0] direction and possessed a specific surface area of 36.1 m^2/g and a large number of nanopores (2–4 nm and 8 nm). The sheaf-like Ga_2O_3 exhibits a remarkable photocatalytic activity and high mineralization rate for PFOA decomposition in pure water under UV irradiation. Bicarbonate and organic matters significantly inhibited the photocatalytic decomposition of PFOA in sewage water. However, in combination with 185 nm VUV light, which had the same electric consumption as 254 nm UV light, the sheaf-like Ga_2O_3 could still fast decompose PFOA in wastewater, which can be attributed to the role of VUV irradiation to eliminate adverse impacts of coexisting organic matters and remarkable activity of the sheaf-like Ga_2O_3 to decompose PFOA. This indicates that the sheaf-like Ga_2O_3/VUV process is a promising method for removing trace PFOA and similar pollutants in real wastewater.

Acknowledgements

This work was financially supported by National Natural Science Foundation of China (21177071), National Basic Research Program of China (2013CB632403) and Science Fund for Creative Research Groups (21221004).

References

[1] M. Clara, C. Scheffknecht, S. Scharf, S. Weiss, O. Gans, Water Science and Technology 58 (2008) 59–66.
[2] J.P. Benskin, L. Yeung, N. Yamashita, S. Taniyasu, P. Lam, J.W. Martin, Environmental Science and Technology 44 (2010) 9049–9054.
[3] H.M. Shin, V.M. Vieira, P.B. Ryan, R. Detwiler, B. Sanders, K. Steenland, S.M. Bartell, Environmental Science and Technology 45 (2011) 1435–1442.
[4] T. Zhang, Q. Wu, H.W. Sun, X.Z. Zhang, S.H. Yun, K. Kannan, Environmental Science and Technology 44 (2010) 4341–4347.
[5] G.P. Zhao, J. Wang, X.F. Wang, S.P. Chen, Y. Zhao, F. Gu, A. Xu, L.J. Wu, Environmental Science and Technology 45 (2011) 1638–1644.
[6] J.H. Yang, Chemosphere 81 (2010) 548–552.
[7] M.M. Schultz, C.P. Higgins, C.A. Huset, R.G. Luthy, D.F. Barofsky, J.A. Field, Environmental Science and Technology 40 (2006) 7350–7357.
[8] H. Moriwaki, Y. Takagi, M. Tanaka, K. Tsuruho, K. Okitsu, Y. Maeda, Environmental Science and Technology 39 (2005) 3388–3392.
[9] R.R. Giri, H. Ozaki, T. Morigaki, S. Taniguchi, R. Takanami, Water Science and Technology 63 (2011) 276–282.
[10] M.H. Cao, B.B. Wang, H.S. Yu, L.L. Wang, S.H. Yuan, J. Chen, Journal of Hazardous Materials 179 (2010) 1143–1146.
[11] B.B. Wang, M.H. Cao, Z.J. Tan, L.L. Wang, S.H. Yuan, J. Chen, Journal of Hazardous Materials 181 (2010) 187–192.
[12] Y. Qu, C.J. Zhang, F. Li, J. Chen, Q. Zhou, Water Research 44 (2010) 2939–2947.
[13] H. Hori, E. Hayakawa, H. Einaga, S. Kutsuna, K. Koike, T. Ibusuki, H. Kiatagawa, R. Arakawa, Environmental Science and Technology 38 (2004) 6118–6124.
[14] Y. Wang, P.Y. Zhang, G. Pan, H. Chen, Journal of Hazardous Materials 160 (2008) 181–186.
[15] J. Cheng, C.D. Vecitis, H. Park, B.T. Mader, M.R. Hoffmann, Environmental Science and Technology 44 (2010) 445–450.
[16] R.R. Giri, H. Ozaki, T. Okada, S. Takikita, S. Taniguchi, R. Takanami, Water Science and Technology 64 (2011) 1980–1986.
[17] R. Dillert, D. Bahnemann, H. Hidaka, Chemosphere 67 (2007) 785–792.
[18] B.X. Zhao, P.Y. Zhang, Catalysis Communications 10 (2009) 1184–1187.
[19] X.Y. Li, P.Y. Zhang, L. Jin, T. Shao, Z.M. Li, J.J. Cao, Environmental Science and Technology 46 (2012) 5528–5534.
[20] Z.M. Li, P.Y. Zhang, T. Shao, Applied Catalysis B 125 (2012) 350–357.
[21] J. Lin, M. Yu, C. Lin, X. Liu, Journal of Physical Chemistry C 111 (2007) 5835–5845.
[22] Z.R. Dai, Z.W. Pan, Z.L. Wang, Advanced Functional Materials 13 (2003) 9–24.
[23] S.C. Yan, L.J. Wan, Z.S. Li, Y. Zhou, Z.G. Zou, Chemical Communications 46 (2010) 6388–6390.
[24] C.C. Huang, C.S. Yeh, New Journal of Chemistry 34 (2010) 103–107.
[25] J. Tang, A.P. Alivisatos, Nano Letters 6 (2006) 2701–2706.
[26] C.D. Vecitis, H. Park, J. Cheng, B.T. Mader, M.R. Hoffmann, Frontiers of Environmental Science & Engineering in China 3 (2009) 129–151.
[27] S. Kutsuna, Y. Nagaoka, K. Takeuchi, H. Hori, Environmental Science and Technology 40 (2006) 6824–6829.
[28] M.I. Franch, J.A. Ayllon, J. Peral, X. Domenech, Catalysis Today 101 (2005) 245–252.

[29] T. van der Meulen, A. Mattson, L. Osterlund, Journal of Catalysis 251 (2007) 131–144.
[30] F.P. Rotzinger, J.M. Kesselman-Truttmann, S.J. Hug, V. Shklover, M. Grätzel, Journal of Physical Chemistry B 108 (2004) 5004–5017.
[31] G.B. Deacon, R.J. Phlips, Coordination Chemistry Reviews 33 (1980) 227–250.
[32] H.G. Yang, C.H. Sun, S.Z. Qiao, J. Zou, G. Liu, S.C. Smith, H.M. Cheng, G.Q. Lu, Nature 453 (2008) 638–641.
[33] G. Liu, J.C. Yu, G.Q. Lu, H.M. Cheng, Chemical Communications 47 (2011) 6763–6783.
[34] S. Kim, J.S. Lee, C. Mitterbauer, Q.M. Ramasse, M.C. Sarahan, N.D. Browning, H.J. Park, Chemistry of Materials 21 (2009) 1182–1186.
[35] G. Imoberdorf, M. Mohseni, Journal of Hazardous Materials 186 (2011) 240–246.
[36] W.Y. Han, P.Y. Zhang, W.P. Zhu, J.J. Yin, L.S. Li, Water Research 38 (2004) 4197–4203.
[37] J. Chen, P.Y. Zhang, J. Liu, Journal of Environmental Sciences (China) 19 (2007) 387–390.